buildings

MDPI

*Article*

# Combined Effects of Steel and Glass Fibres on the Fracture Performance of Recycled Rubber Concrete

**Xiaohui Li [1], Zezhou Pan [1], Hao Zhen [1], Wenhua Luo [1], Zhuangwei Chen [2], Hongming Li [3], Zhichao Wu [3], Feng Liu [1] and Lijuan Li [1,*]**

[1] School of Civil and Transportation Engineering, Guangdong University of Technology, Guangzhou 510006, China
[2] Guangdong Henghui Construction Group Co., Ltd., Guangzhou 510006, China
[3] Guangdong Zhongdu Construction Group Co., Ltd., Lianjiang 524499, China
* Correspondence: lilj@gdut.edu.cn

**Abstract:** As an environmentally friendly construction material, recycled rubber concrete (RRC) is commonly used as a road material owing to its excellent flexural strength and crack resistance. Previous studies have shown that the addition of fibres is an effective method for improving the crack resistance of concrete. The purpose of this study is to investigate the fracture performance of RRC reinforced with steel fibres (SFs) and glass fibres (GFs). A total of 28 RRC mixtures were prepared. The results of the fracture test showed that the addition of SFs and GFs significantly enhanced the RRC fracture performance. The maximum increases or decreases in flexural strength, brittleness coefficient, fracture energy, initial fracture toughness, and unstable fracture toughness were 64.9, −34.6, 775.6, 92.0, and 118.4%, respectively. The ideal GF content is usually in the range of 0.4–0.6% and decreases with increasing SF content. In addition, scanning electron microscope (SEM) tests were conducted to explore the mechanism of the effect of hybrid fibres on RRC at a microscopic level. The results show that SFs were always pulled out, while GFs were pulled apart at the initial defects. At the same time, excessive GFs caused more initial defects. These results are expected to provide theoretical direction and experimental support for the practical application of hybrid fibre-reinforced recycled rubber concrete (HFRRRC).

**Keywords:** fracture performance; steel fibres; glass fibres; hybrid fibres; recycled rubber concrete

check for updates

**Citation:** Li, X.; Pan, Z.; Zhen, H.; Luo, W.; Chen, Z.; Li, H.; Wu, Z.; Liu, F.; Li, L. Combined Effects of Steel and Glass Fibres on the Fracture Performance of Recycled Rubber Concrete. *Buildings* **2024**, *14*, 864. https://doi.org/10.3390/buildings14040864

Academic Editor: Marco Di Ludovico

Received: 17 February 2024
Revised: 16 March 2024
Accepted: 21 March 2024
Published: 22 March 2024



## 1. Introduction

The widespread use of traditional concrete has led to excessive exploitation of natural aggregates, which exacerbates the depletion of natural resources and environmental damage. Therefore, many researchers propose using recycled resources and abundant sea sand resources as alternatives [1,2]. Meanwhile, with the development of urbanisation, the number of means of transportation is growing rapidly. This not only requires high-quality road materials, but also produces more waste rubber from scrapped car tires. Waste rubber cannot be degraded naturally. Moreover, waste tires are difficult to dissolve at high temperatures; therefore, it is very difficult for waste tires to be recycled into new rubber products. The most common disposal options for waste rubber tires are direct burning and burial, both of which cause irreversible pollution of the natural environment. To overcome the negative impact of waste rubber on the environment, there is an urgent need to develop a harmless method for consuming large quantities of waste rubber [3]. The use of recycled rubber (RR) in the concrete industry is an attempt to move in this direction. The use of RR as a substitute aggregate not only reduces the environmental impact of waste rubber by consuming it in large quantities, but also significantly reduces the consumption of natural aggregates such as sand and gravel [4–6]. The use of RR in the concrete industry has been attempted for a long time. However, it has been found that some of the key mechanical properties of concrete, including workability, compressive strength, tensile strength, stiffness, and modulus of elasticity, are significantly reduced when rubber is added to concrete [7–9]. Because road materials require a lower modulus of elasticity to improve the comfort of vehicle occupants, the decline in these properties makes recycled rubber concrete (RRC) an ideal road material [10,11]. Furthermore, RRC has a higher energy dissipation capacity than ordinary concrete, which makes it more resistant to vehicle impact loads as a road material [12,13].

Strength, stiffness, and stability are three key factors to consider when designing a structure [14,15]. While it is difficult to improve mechanical properties at the structural level, improving them at the material level is an effective approach. In recent years, more and more new types of high-performance concrete have been studied [16–18]. Concrete pavements are typically damaged by cracking owing to excessive bending and tensile stresses, as concrete itself is a material with good compressive properties and poor fracture properties. Therefore, numerous researchers have explored methods to improve the mechanics properties of RRC [19–21]. One effective method to improve the fracture properties of concrete is to add fibres within the concrete [22–25]. From a comprehensive perspective, the incorporation of fibres can significantly enhance the fracture properties of concrete; however, the enhancement effect of different fibres varies. Overall, the improvement in the fracture performance of concrete by fibres mainly depends on the following three aspects: (1) the type and characteristics of fibres, (2) the direction and distribution of fibres, and (3) the bond between the fibres and the cement matrix. Regarding the types and characteristics of fibres, the selection of fibres with a higher tensile strength and elasticity modulus is beneficial for enhancing the fracture properties of concrete [26,27]. Finer and softer fibres mainly limit the development of microcracks into macroscopic cracks, whereas larger and stiffer fibres mainly limit the development of macroscopic cracks and reduce the crack width [28,29]. Therefore, the addition of hybrid fibres is more effective in improving the fracture properties of concrete. With respect to the direction and distribution of fibres, the fracture resistance of each part within the concrete was enhanced when the fibre material was uniformly distributed within the concrete, thus improving the overall fracture resistance of the concrete. When the direction of the fibre was parallel to the direction of the main tensile stress in the concrete, the fibres effectively improved the crack resistance of the concrete. The direction and distribution of the fibre material within the concrete are mainly related to the workability of the fresh concrete, casting process, size of the specimen, and wall effect of the formwork [30]. Wang et al. studied the strengthening effect of four types of fibres on the fracture performance of rubber concrete. Compared with the control group, all fibres significantly enhanced fracture energy and crack propagation after cracking. Among them, steel fibres (SFs) are the best, increasing the fracture energy by about 50 times. The pull-out resistance of different fibres is not affected by the addition of rubber [31]. Gültekin et al. studied the fracture energy, compressive strength, and flexural strength of self compacting concrete, including glass fibres (GFs) or basalt fibres. Although the addition of fibres usually reduces compressive strength, it significantly improves flexural strength and fracture energy. The flexural strength and fracture energy of glass fibre reinforced concrete have been increased by 58.6% and 55.1%, respectively [32]. Muhyaddin studied the hybridisation of GF, micro steel fibre (MSF) and long hooked steel fibre (HSF) to improve the mechanical and fracture properties of ultra-high performance concrete (UHPC). The results show that the performance order is MSF+HSF, MSF+GF, and HSF+GF. The use of a single GF does not improve ductility and may even exhibit brittle failure [33]. In addition, excessive fibre addition not only tends to cause fibre agglomeration, but also weakens the bond interface between the fibres and concrete [34]. Therefore, although the addition of fibres enhances the fracture properties of concrete, the type, characteristics, and content of fibres need to be carefully selected to maximise their role.

At present, there is limited research on the fracture performance of SF and GF reinforced concrete, especially on RRC. Compared to ordinary concrete, RRC often has more internal defects, and the mechanism of the fibre-combined effect in RRC needs to be explored. This is significant for improving the crack resistance performance of rubber concrete pavement, thereby increasing the service life of the pavement. Therefore, this study investigated the fracture performance of RRC containing SFs and GFs, and analysed the influence mechanism of SF and GF on the fracture performance of RRC through microscopic experiments. The results of this research provide important guidelines for producing and using RRC.

## 2. Experimental Setup

### *2.1. Raw Materials*

In this study, the strength grade and specific gravity of ordinary Portland cement were 42.5R and 3.11, respectively. The properties of cement are shown in Table 1. The experimental water was tapping water from Guangdong University of Technology, with a specific gravity of 1.00. River sand with a maximum particle size of 5 mm and 20 mesh waste rubber were used as fine aggregates. Table 2 shows the river sand parameters obtained according to GB/T14684-2011 [35]. The parameters of the RR provided by the recycled rubber production company are shown in Table 2. The coarse aggregate was made of granite crushed stone with a particle size of 5–16 mm. Table 2 shows the coarse aggregates parameters obtained according to GB/T14685-2011 [36]. The gradation distributions of the sand, RR, and coarse aggregates obtained through the screening test are shown in Figure 1. A straight copper-plated SF with a length of 12 mm was used according to the parameters provided by the supplier. Two lengths of GFs were used in this study, which were 6 and 12 mm. The physical parameters of the fibres are listed in Table 3. Finally, the superplasticiser (SP) was used to enhance the workability of RRC. The solid content and specific gravity of the SP were 9% and 1.02, respectively.

**Table 1.** The properties of cement.

| Contents | CaO | $SiO_2$ | $Fe_2O_3$ | $Al_2O_3$ | $SO_3$ | MgO | Fineness | Loss on Ignition |
|---|---|---|---|---|---|---|---|---|
| Composition (%) | 63–67 | 19–23 | 4–6 | 3–7 | 1.9 | 1 | 1.1 | 1.7 |

**Table 2.** The basic performance of fine and coarse aggregates.

| Aggregate Type | Particle Size (mm) | Apparent Density (kg/m$^3$) | Bulk Density (kg/m$^3$) | Water Absorption (%) |
|---|---|---|---|---|
| Sand | <5 | 2636 | 1543 | 0.5 |
| Recycled rubber | <2.5 | 750 | - | - |
| Coarse aggregate | 5–16 | 2641 | 1344 | 2.1 |

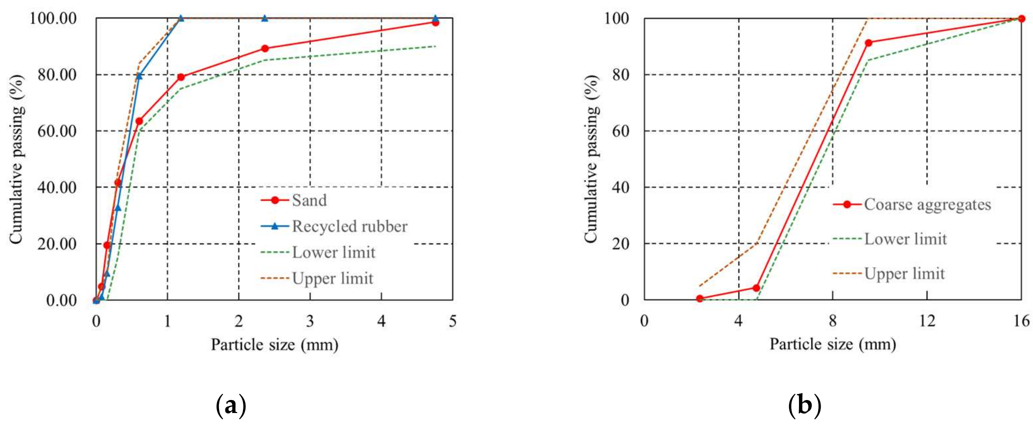


**Figure 1.** Passing rate of aggregates: (**a**) fine aggregates; (**b**) coarse aggregates.

**Table 3.** Properties of SFs and GFs.

| Fibre Type | Length (mm) | Specific Gravity | Equivalent Diameter (μm) | Tensile Strength (MPa) | Elastic Modulus (GPa) |
|---|---|---|---|---|---|
| Steel fibres (SFs) | 12 | 7.8 | 200 | 3000 | 200 |
| Glass fibres (GFs) | 6/12 | 2.68 | 14 | 1700 | 72 |

### 2.2. Concrete Mixtures

To explore the anti-cracking and toughening effects of SF and GF on the fracture performance of RRC, 28 mix proportions were designed in this study, as shown in Table 4. Fibres were added according to the volume percentage of concrete. The content of SFs was designed as 0, 0.4%, 0.8% and 1.2%, and the content of GFs was designed as 0, 0.2%, 0.4% and 0.6%. In this study, rubber content was set to 10%. RR was added according to the volume percentage of the fine aggregate. The SP was added according to the mass percentage of the cement, which was 0.5% in this study. The water-cement ratio was 0.4, and water consumption was adjusted based on the moisture content and water absorption of the aggregates. Each mix proportion is marked in the SxGyLz format. Sx indicates that the SF content is x%. Similarly, Gy indicates that the GF content is y%. Lz is the length of the GFs, which is z mm. If the mix number is without Lz, this implies that no GFs have been added.

**Table 4.** Test mixture (kg/m$^3$).

| Mix Number | Cement | Water | GFs | SFs | Coarse Aggregate | Sand | Recycled Rubber | SP |
|---|---|---|---|---|---|---|---|---|
| S0G0 | 554.10 | 245.30 | 0.00 | 0.00 | 966.30 | 531.20 | 17.10 | 2.80 |
| S0.4G0 | 551.90 | 244.40 | 0.00 | 31.20 | 962.40 | 529.10 | 17.00 | 2.80 |
| S0.8G0 | 549.70 | 243.40 | 0.00 | 62.40 | 958.50 | 527.00 | 16.90 | 2.80 |
| S1.2G0 | 547.50 | 242.40 | 0.00 | 93.60 | 954.70 | 524.80 | 16.90 | 2.70 |
| S0G0.2L6 | 553.00 | 244.90 | 5.40 | 0.00 | 964.30 | 530.20 | 17.00 | 2.80 |
| S0.4G0.2L6 | 550.80 | 243.90 | 5.40 | 31.20 | 960.50 | 528.00 | 17.00 | 2.80 |
| S0.8G0.2L6 | 548.60 | 242.90 | 5.40 | 62.40 | 956.60 | 525.90 | 16.90 | 2.70 |
| S1.2G0.2L6 | 546.40 | 241.90 | 5.40 | 93.60 | 952.70 | 523.80 | 16.80 | 2.70 |
| S0G0.4L6 | 551.90 | 244.40 | 10.70 | 0.00 | 962.40 | 529.10 | 17.00 | 2.80 |
| S0.4G0.4L6 | 549.70 | 243.40 | 10.70 | 31.20 | 958.50 | 527.00 | 16.90 | 2.80 |
| S0.8G0.4L6 | 547.50 | 242.40 | 10.70 | 62.40 | 954.70 | 524.80 | 16.90 | 2.70 |
| S1.2G0.4L6 | 545.20 | 241.40 | 10.70 | 93.60 | 950.80 | 522.70 | 16.80 | 2.70 |
| S0G0.6L6 | 550.80 | 243.90 | 16.10 | 0.00 | 960.50 | 528.00 | 17.00 | 2.80 |
| S0.4G0.6L6 | 548.60 | 242.90 | 16.10 | 31.20 | 956.60 | 525.90 | 16.90 | 2.70 |
| S0.8G0.6L6 | 546.40 | 241.90 | 16.10 | 62.40 | 952.70 | 523.80 | 16.80 | 2.70 |
| S1.2G0.6L6 | 544.10 | 240.90 | 16.10 | 93.60 | 948.90 | 521.70 | 16.70 | 2.70 |
| S0G0.2L12 | 553.00 | 244.90 | 5.40 | 0.00 | 964.30 | 530.20 | 17.00 | 2.80 |
| S0.4G0.2L12 | 550.80 | 243.90 | 5.40 | 31.20 | 960.50 | 528.00 | 17.00 | 2.80 |
| S0.8G0.2L12 | 548.60 | 242.90 | 5.40 | 62.40 | 956.60 | 525.90 | 16.90 | 2.70 |
| S1.2G0.2L12 | 546.40 | 241.90 | 5.40 | 93.60 | 952.70 | 523.80 | 16.80 | 2.70 |
| S0G0.4L12 | 551.90 | 244.40 | 10.70 | 0.00 | 962.40 | 529.10 | 17.00 | 2.80 |
| S0.4G0.4L12 | 549.70 | 243.40 | 10.70 | 31.20 | 958.50 | 527.00 | 16.90 | 2.80 |
| S0.8G0.4L12 | 547.50 | 242.40 | 10.70 | 62.40 | 954.70 | 524.80 | 16.90 | 2.70 |
| S1.2G0.4L12 | 545.20 | 241.40 | 10.70 | 93.60 | 950.80 | 522.70 | 16.80 | 2.70 |
| S0G0.6L12 | 550.80 | 243.90 | 16.10 | 0.00 | 960.50 | 528.00 | 17.00 | 2.80 |
| S0.4G0.6L12 | 548.60 | 242.90 | 16.10 | 31.20 | 956.60 | 525.90 | 16.90 | 2.70 |
| S0.8G0.6L12 | 546.40 | 241.90 | 16.10 | 62.40 | 952.70 | 523.80 | 16.80 | 2.70 |
| S1.2G0.6L12 | 544.10 | 240.90 | 16.10 | 93.60 | 948.90 | 521.70 | 16.70 | 2.70 |

### 2.3. Preparation of Test Specimens

Beams with lengths ($l$), widths ($t$), and heights ($h$) of 400, 100, and 100 mm, respectively, were used as fracture specimens [37]. The height ($a_0$) and width of the pre-cracks were 30 and 1 mm, respectively. A schematic diagram of the size of the specimen is shown in Figure 2. Three beams with pre-cracks were prepared for each mix proportion as fracture specimens, for a total of 84. To obtain the compressive strength, three cylinders with diameters of 100 mm and heights of 200 mm were prepared for each mix proportion as axial compression specimens.

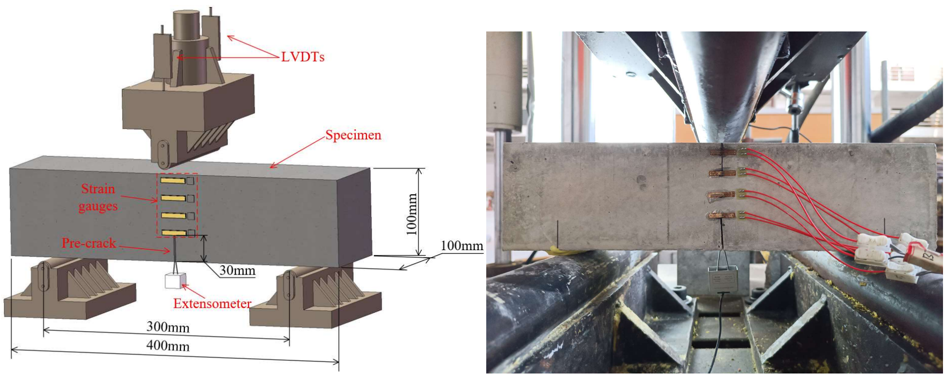


**Figure 2.** Test setups of the fracture test.

The preparation process of specimens is shown in Figure 3. To evenly distribute the GFs and SFs within the RRC, the preparation process of hybrid fibre-reinforced recycled rubber concrete (HFRRRC) is divided into eight steps. (1) First, cement, sand, and RR were added to a mixer for dry mixing. After starting the mixer, SFs and GFs were uniformly added, which lasted for 60 s. (2) After water and SP were fully mixed, around 70% of the mixture was poured to the mixer and operated for 60 s. (3) The remaining 30% mixture and coarse aggregates were poured into the mixer, and operated the mixer for 180 s to thoroughly mix it. (4) Fresh concrete was poured into the moulds and vibrated for 1 min. The vibration time should not be excessively long to prevent the SF from sinking to the bottom and the rubber particles from floating. (5) Aluminium sheets with a thickness of 1 mm were vertically inserted into the fresh concrete to form a pre-crack. (6) Fresh concrete was smoothened along the surface of the test mould. To prevent the evaporation of internal water and to affect the hydration rate of the cement, the specimens were covered tightly with plastic and wet linen cloths. (7) After the initial setting of the fresh concrete, the aluminium sheets were carefully pulled out with iron tongs. (8) After curing for 24 h, the specimens were demoulded and cured in water for 28 days. Finally, the specimens were removed and wiped dry before mechanical testing.

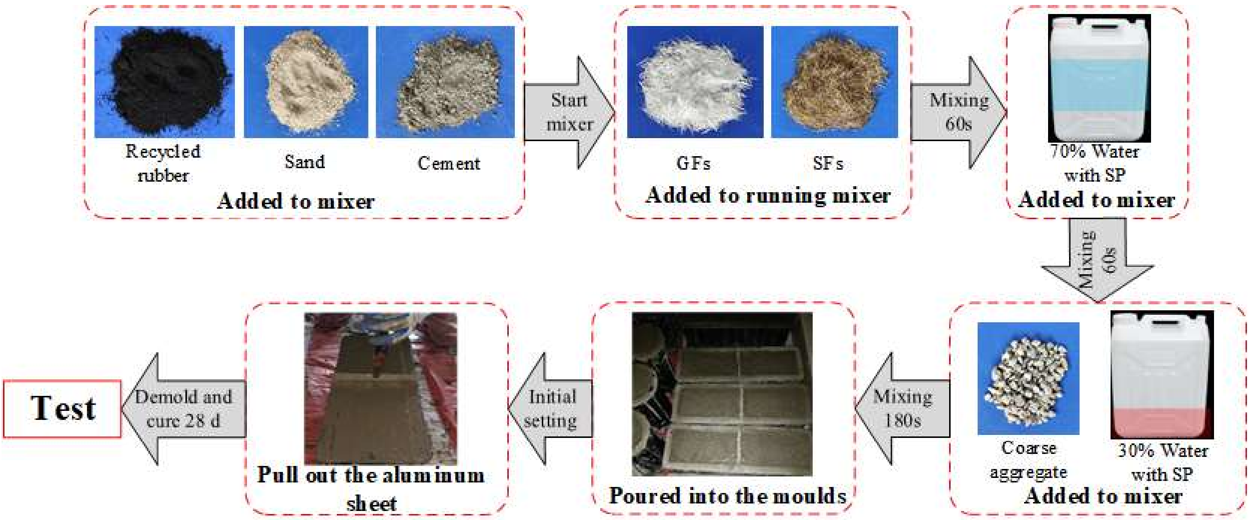


**Figure 3.** The preparation process of specimens.

## *2.4. Testing Schemes*

Axial deformation in the axial compression test was measured using two linear variable differential transformers (LVDTs). The LVDTs were mounted in the middle of the specimen at a distance of 80 mm. The loading procedure for the compression experiments was displacement controlled, which was 0.18 mm/min. The compressive strength of each specimen was determined according to the standard ASTM C39/C39M [38].

An electro-hydraulic servo static and dynamic universal testing machine with a maximum capacity of 500 kN was used for the fracture tests. The fracture test setup is illustrated in Figure 2. The support span, $s$, was 300 mm. Two LVDTs were symmetrically placed in the mid span of the test specimens to measure the deflection. Four strain gauges were used to test the crack development in each specimen. Crack mouth opening displacement (CMOD) was measured using an extensometer. To fix the extensometer, two aluminium sheets with a thickness ($h_0$) of 1 mm were symmetrically bonded to both sides of the pre-crack using an adhesive. To eliminate load eccentricity, the top and bottom of the specimens were levelled with high-strength gypsum before the test. A load was applied with a displacement control of 0.2 mm/min. During the test, strain gauges, LVDTs, extensometer, and load data were recorded at a frequency of 1 Hz.

The analysis indices of the fracture test included the flexural strength $f_t$, fracture energy $G_f$, initial fracture toughness $K^{ini}$, and unstable fracture toughness $K^{un}$. The flexural strength of the specimens was calculated as follows:

$$f_t = \frac{3P_{max}s}{2t(h-a_0)^2} \tag{1}$$

where $P_{max}$ is the maximum load during the testing. The equation for calculating the fracture energy $G_f$ is as follows:

$$G_f = \frac{\int_0^{\delta_0} P\mathrm{d}\delta + mg\frac{s}{l}\delta_0}{t(h-a_0)} \tag{2}$$

where $P$ is the load recorded during the test; $\delta_0$ is the deflection required for calculating the fracture energy and is determined as 2 mm; m represents the mass of the specimen; $g$ is the gravitational acceleration, i.e., 9.8 N/kg.

In this study, fracture toughness was calculated using the double-K fracture criterion proposed by Xu and Reinhardt [39]. According to this criterion, the initial fracture toughness and unstable fracture toughness are the key indicators for determining the fracture performance of concrete. When the stress intensity factor of concrete was less than the initial fracture toughness, cracks did not develop. When the stress intensity factor was greater than the initial fracture toughness and less than the unstable fracture toughness, cracks developed stably. Crack instability develops when the stress intensity factor exceeds the unstable fracture toughness. Therefore, the crack toughness can be calculated as follows:

$$K^{ini} = \frac{3P_{ini}s}{2h^2t}\sqrt{a_0}F\left(\frac{a_0}{h}\right) \tag{3}$$

$$F\left(\frac{a_0}{h}\right) = \frac{1.99 - \frac{a_0}{h}\left(1-\frac{a_0}{h}\right)\left(2.15 - \frac{3.93a_0}{h} + 2.7\left(\frac{a_0}{h}\right)^2\right)}{\left(1+2\frac{a_0}{h}\right)\left(1-\frac{a_0}{h}\right)^{\frac{3}{2}}} \tag{4}$$

where $F(a_0/h)$ is calculated using Equation (4). $P_{ini}$ denotes cracking load. Determining the initial load is key to processing the test data, and there are generally two methods. The first is the strain gauge method [40,41]. The strain gauges are pasted on both sides of the pre-crack end, and the retraction point of the strain value of the load–strain curve is considered as the cracking point. This method is simple, easy to implement, and widely used. The second method is the test curve method [37,42]. As stated in the standard and other studies, the load corresponding to the turning point of the rising section of the load–CMOD curve from a straight section to a curved section is the cracking load. This method can overcome some of the disadvantages of the strain gauge method (e.g., the appearance times of surface cracks and internal cracks are inconsistent). In this study, the second method is used to determine the cracking point.

To calculate the unstable fracture toughness, the initiation load $P_{\mathrm{ini}}$ and pre-crack height $a_0$ in Equations (3) and (4) were replaced with the maximum load $P_{\max}$ and critical crack length $a_c$, respectively. The critical crack length was calculated as follows:

$$a_c = \frac{2}{\pi}(h + h_0)\arctan\sqrt{\frac{tE_f}{32.6P_{\max}}\mathrm{CMOD}_c - 0.1135} - h_0 \quad (5)$$

where $h_0$ is the thickness of the aluminium sheet; $\mathrm{CMOD}_c$ is the CMOD corresponding to the maximum load $P_{\max}$; $E_f$ is the rupture modulus, which was calculated as:

$$E_f = \frac{1}{tc_i}\left[3.70 + 32.6\tan^2\left(\frac{\pi}{2}\frac{a_0 + h_0}{h + h_0}\right)\right] \quad (6)$$

where $c_i$ denotes the initial compliance. This was calculated as the ratio of $P$ to CMOD at any point on the straight segment of the $P$–CMOD curve. $P_{\mathrm{ini}}$ and its corresponding CMOD were selected uniformly for this study.

Finally, samples were obtained from the fracture surface of the specimen for the scanning electron microscope (SEM) test.

## 3. Result and Discussion

### *3.1. Failure Mode Analysis*

The final morphologies of the fractured specimens are shown in Figure 4. For the specimens without SFs, as shown in the left column of Figure 4, the cracks mostly developed vertically upward after they appeared, and the crack widths were not large. When the GF content was 0.6%, as shown in Figure 4m,y, the development path of the cracks became more tortuous. This indicates that when SFs were not added, the macroscopic cracks were not effectively confined and always developed along the high-stress position. Further, a small crack width indicates that the deformation of the specimen was small when its failure and the deformation ability was poor. Specimens with different SF contents are shown in the rows in Figure 4. With the increase in SF content, the crack above pre-crack changes from vertical to tortuous. This indicates that the presence of SFs can enhance the crack resistance of RRC so that crack development avoids these enhanced areas. In addition, the crack width increased with increasing SF content. This indicates that the deformation during the RRC fracture failure was larger, and the deformation capacity was better with the increase in the SF content.

According to the failure mode analysis, the effects of the two fibres on the fracture performance of the RRC are as follows: When only the GFs were added, the cracks in the specimens were relatively vertical. This shows that GF had little effect on the restriction of macroscopic cracks, and the cracks appeared at the position of the greatest stress. The GFs that appeared in the macroscopic cracks were either pulled out or broken. Therefore, the GFs mainly acted before the appearance of macroscopic cracks. Whether it was a 6 mm or 12 mm GF, it had no significant effect on the final failure mode of the fracture specimen. In contrast, SFs had a greater influence on the final failure mode. The main reason for this was that the bridging effect of SFs can continue after the appearance of macroscopic cracks. Steel fibres reduce the maximum stress at the crack tip by altering the strain field at the crack tip. Studies have shown that as long as the crack width does not exceed 1/4 of the length of the SF, SF-reinforced concrete still has a load-bearing capacity [43]. Therefore, SFs can improve the deformation ability and toughness of RRC.

Figure 5 shows the crack development in fracture tests. At the beginning, as shown in Figure 5a, the fibres are uniformly distributed in the RRC and there is a number of initial defects. As the load increases, microcracks first appear at initial defects and the interface between the aggregates and matrix, as shown in Figure 5b. At this point, GFs can suppress the development of microcracks. When the load continues to increase to the cracking load, microcracks connect to form macroscopic cracks. Cracks usually avoid fibres and appear in weak areas of RRC. Therefore, the presence of SFs makes macroscopic cracks more tortuous, as shown in Figure 5c. Finally, as shown in Figure 5d, the load continued to increase until it approached the ultimate load of the specimen. At this point, most GFs break, some of SFs are pulled out and fail. Only a portion of SFs play a bridging role. The development time from Figure 5c to 5d is relatively long. In other words, the SFs gradually improve the fracture toughness of RRC during the process of being pulled out.

### 3.2. Load–Deflection Curves

Figure 6 illustrates the load–deflection curves of different series. The load–deflection curves for each series were divided into ascending and descending sections. The influence of SFs and GFs on the load–deflection curves of each series was mainly reflected in the peak load and deformation capacity.

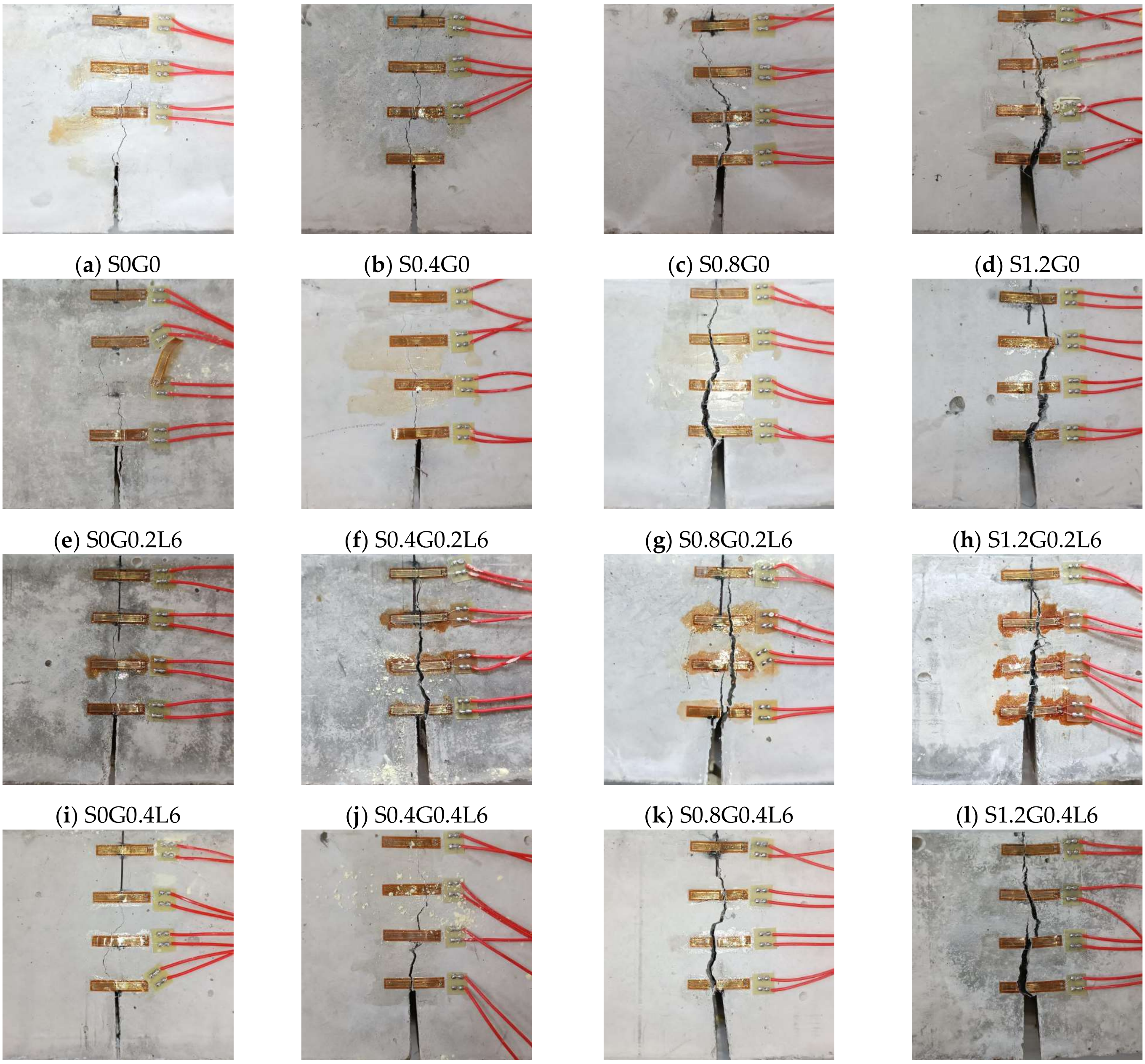

(**a**) S0G0 (**b**) S0.4G0 (**c**) S0.8G0 (**d**) S1.2G0

(**e**) S0G0.2L6 (**f**) S0.4G0.2L6 (**g**) S0.8G0.2L6 (**h**) S1.2G0.2L6

(**i**) S0G0.4L6 (**j**) S0.4G0.4L6 (**k**) S0.8G0.4L6 (**l**) S1.2G0.4L6

**Figure 4.** *Cont*.

(**m**) S0G0.6L6 (**n**) S0.4G0.6L6 (**o**) S0.8G0.6L6 (**p**) S1.2G0.6L6

(**q**) S0G0.2L12 (**r**) S0.4G0.2L12 (**s**) S0.8G0.2L12 (**t**) S1.2G0.2L12

(**u**) S0G0.4L12 (**v**) S0.4G0.4L12 (**w**) S0.8G0.4L12 (**x**) S1.2G0.4L12

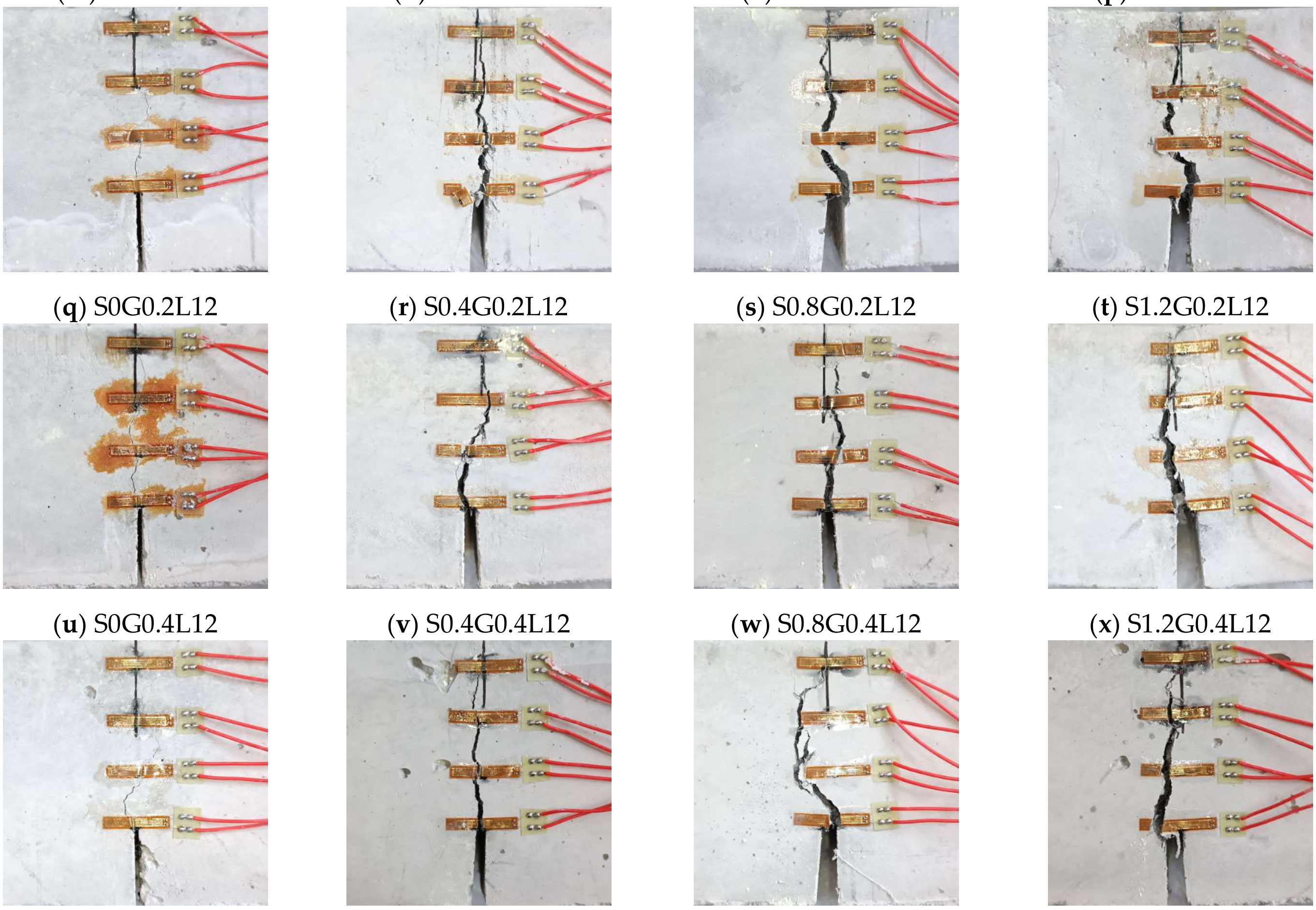

(**y**) S0G0.6L12 (**z**) S0.4G0.6L12 (**aa**) S0.8G0.6L12 (**ab**) S1.2G0.6L12

**Figure 4.** Failure modes of HFRRRC.

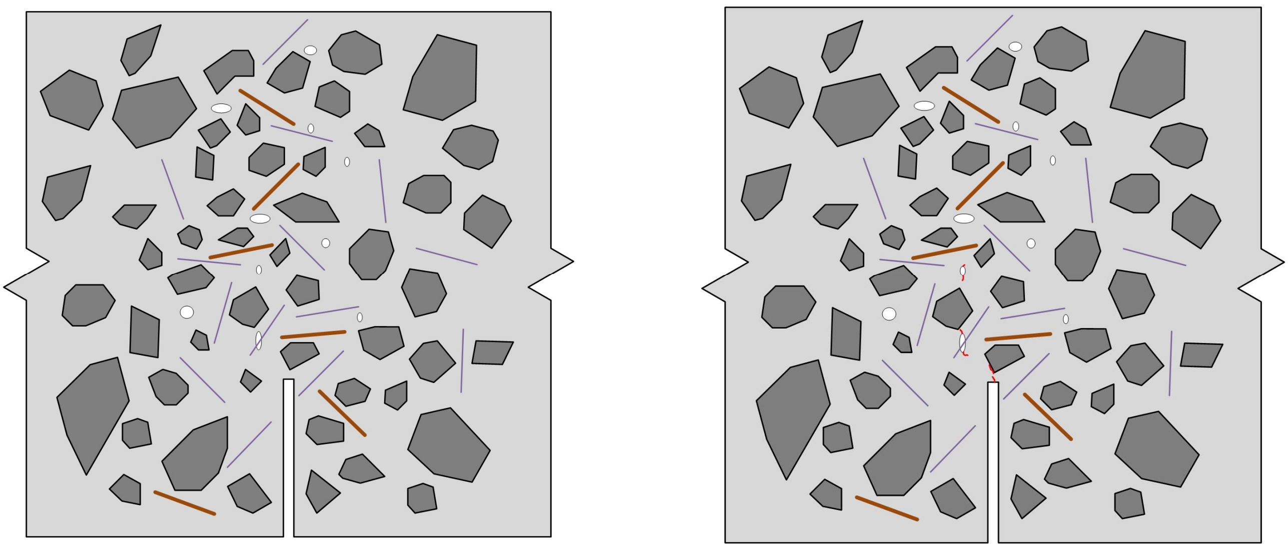

(**a**) (**b**)

**Figure 5.** *Cont.*

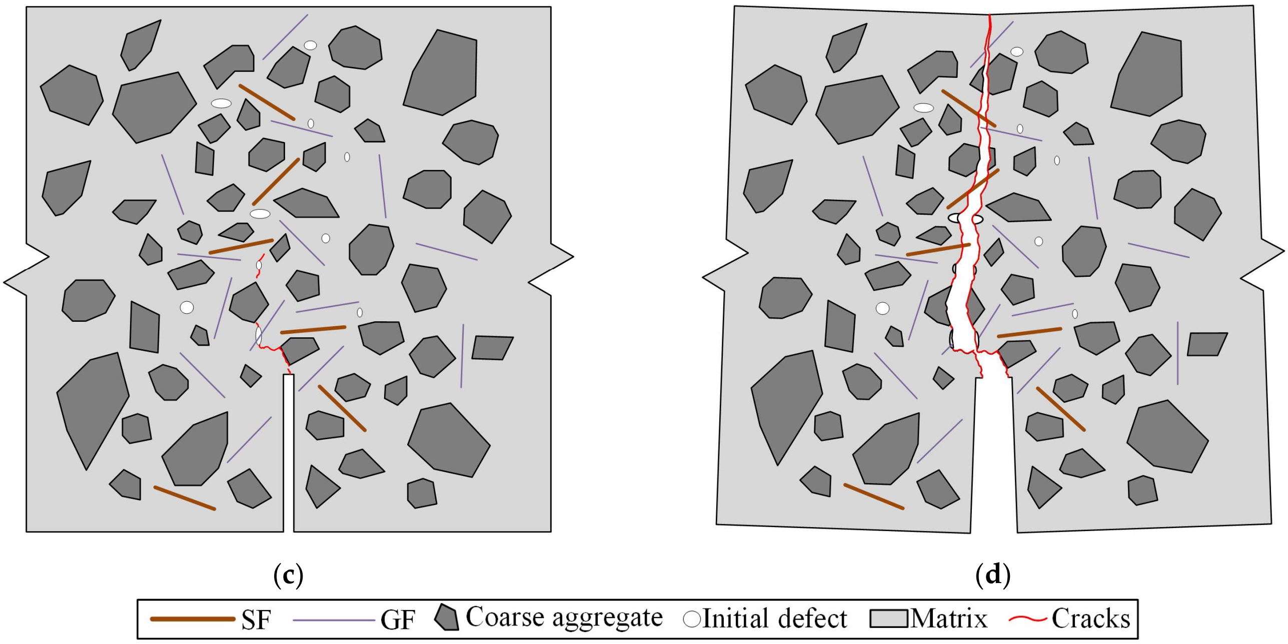


**Figure 5.** Schematic diagram of cracks development in HFRRRC: (**a**) initial state; (**b**) the microcracks appeared; (**c**) the microcracks developed into macrocracks; (**d**) final state.

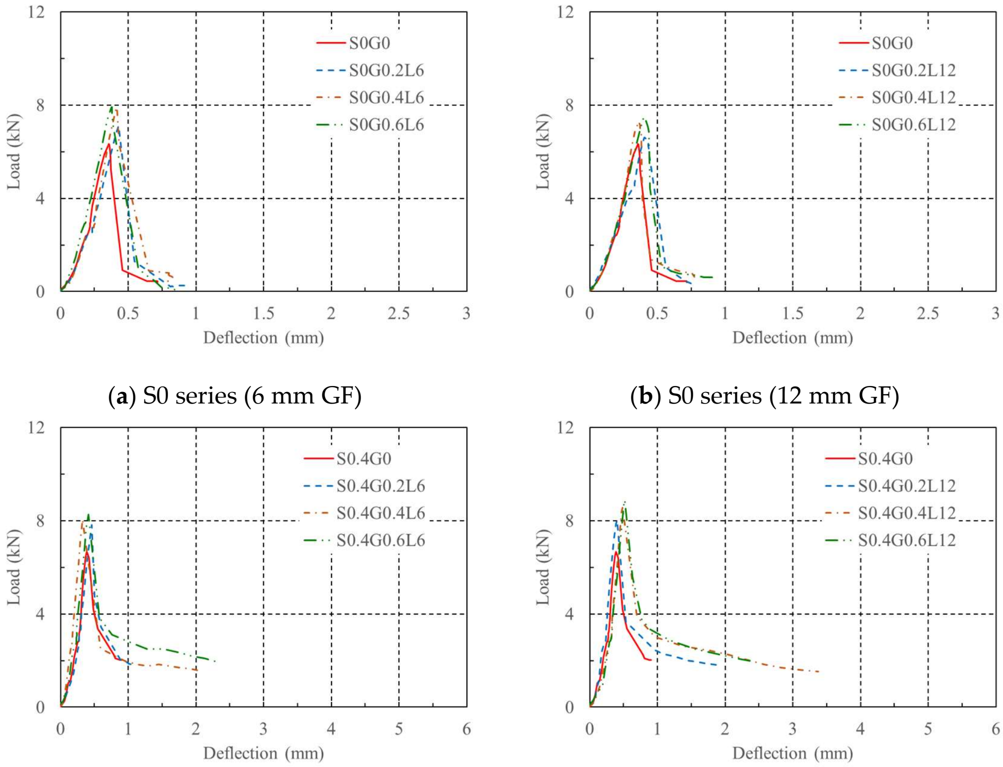


(**a**) S0 series (6 mm GF) (**b**) S0 series (12 mm GF)

(**c**) S0.4 series (6 mm GF) (**d**) S0.4 series (12 mm GF)

**Figure 6.** *Cont*.

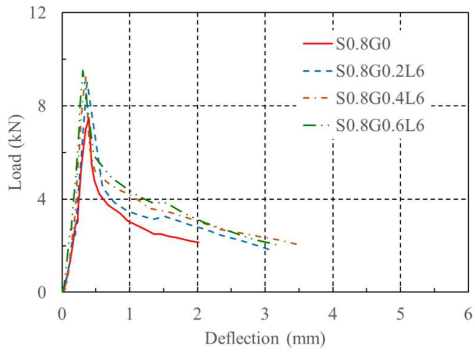


(**e**) S0.8 series (6 mm GF)

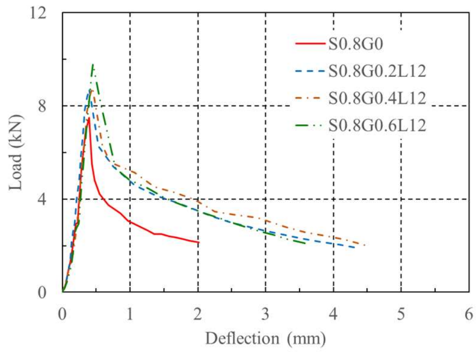


(**f**) S0.8 series (12 mm GF)

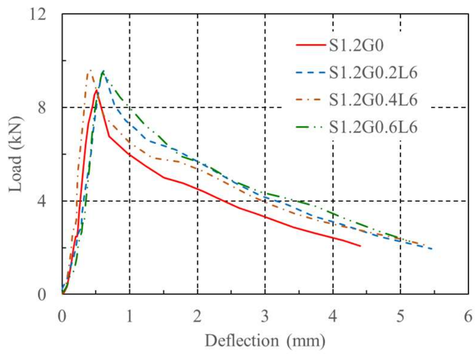


(**g**) S1.2 series (6 mm GF)

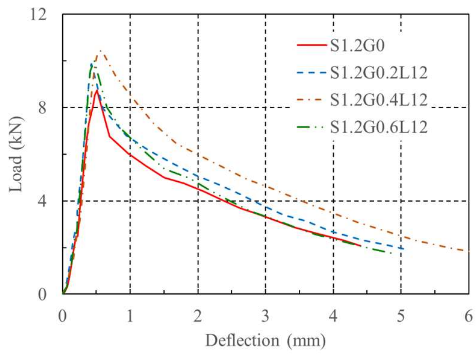


(**h**) S1.2 series (12 mm GF)

**Figure 6.** Load–deflection curves of fracture tests.

From the perspective of the peak load, when the SF content was less than 1.2%, the peak load of the curves increased with the increase in GF content. In this case, when the GF contents of 6 and 12 mm was 0.6%, the peak load was maximised. When the SF content was 1.2%, the peak load of the curves first increased and then decreased as the GF content increased. When the GF content of 6 and 12 mm was 0.4%, the peak load reached its maximum. Therefore, an appropriate amount of GF can increase the peak load. This was because the GFs had a bridging effect and improved the mechanical properties of concrete. However, excessive GFs reduce the workability of fresh concrete and increase the void ratio inside the concrete, which was harmful to the mechanical properties of concrete. When comparing the load–deflection curves for different SF contents, the peak load increases with the increase in SF content. This was because the SFs can play a bridging role after the concrete had cracked so that the concrete on both sides of the crack can continue to carry loads.

The inclusion of fibres can effectively improve the deformation ability of RRC. The deflection corresponding to the peak load was defined as the peak deflection. As shown in Figure 5a,b, when no SF was added, the peak deflection first increases and then decreases with the increase in GF content. The peak deflections of the specimens with GFs were greater than those of the S0G0 group. Both GF lengths had the highest peak deflection when the content was 0.2%. After the peak deflection, the load value decreased rapidly, indicating brittle failure, and the slope of the descending curve was similar to that of the S0G0 group. This indicates that an appropriate number of GFs can improve the deformation capacity of the RRC before the peak load, but there was not much improvement in the deformation capacity after the peak load. This was due to the fact that GFs can limit the formation and development of microcracks in the ascending section of the load–deflection curve. However, excessive GFs can increase the initial defects of the RRC. During the descending section of the load–deflection curve, there were evident macroscopic cracks in the RRC, and the GFs broke or were pulled out to fail. Therefore, the deformation ability of the RRC after the peak load was not significantly improved when only GFs were added. As shown in Figure 5c–f, for the specimens with SFs, the descending section of the load–deflection curve can be divided into two sub-phases: a rapid descent phase and a stabilisation phase. As the SF content increases, the transition zone between these two subphases becomes smoother. The load corresponding to the transition zone was greater. This indicates that SFs can effectively limit the speed of the development of macroscopic cracks. The transition from the rapid descent phase to the stabilisation phase at higher load levels increased the energy consumed and improved the toughness of the RRC. By comparing the 6 mm GFs series with the 12 mm GFs series, it can be observed that the existence of SFs better improves the deformation capacity of the 12 mm GFs series after peak loading.

### 3.3. Index Analysis

Table 5 lists the values of each index. The values of each index in Table 5 represent the average values of the three specimens. If the following two situations occur, they were considered separately: (1) if both the maximum and minimum values differ from the median value by more than 15% of the median value, the median value was considered as the representative value; and (2) if only one of the maximum and minimum values differs from the median value by more than 15% of the median value, the value with a large difference was discarded, and the average of the other two values was considered as the representative value. In addition, to better reflect the impact of SFs and GFs on the indexes, Table 5 also lists the change rates of each index. The rates of change were relative to the S0G0 group. Positive values indicate an increase and negative values indicate a decrease. In addition, because we had previously studied the compressive strength and elastic modulus, this study focuses on the effects of SFs and GFs on the fracture index of RRC.

**Table 5.** Test results.

| Mix Number | Compressive Strength | | Flexural Strength | | Brittleness Coefficient | | Fracture Energy | | Initial Fracture Toughness | | Unstable Fracture Toughness | |
|---|---|---|---|---|---|---|---|---|---|---|---|---|
| | RV * (MPa) | PC * (%) | RV (MPa) | PC (%) | RV | PC (%) | RV (J/m$^2$) | PC (%) | RV (MPa·m$^{1/2}$) | PC (%) | RV (MPa·m$^{1/2}$) | PC (%) |
| S0G0 | 34.36 | - | 5.81 | - | 5.91 | - | 228 | - | 0.60 | - | 1.24 | - |
| S0.4G0 | 36.93 | 7.5 | 6.13 | 5.5 | 6.03 | 1.92 | 405 | 77.3 | 0.79 | 30.2 | 1.74 | 40.3 |
| S0.8G0 | 35.06 | 2.0 | 6.87 | 18.3 | 5.10 | −13.7 | 917 | 301.7 | 0.88 | 46.1 | 2.29 | 84.8 |
| S1.2G0 | 38.09 | 10.9 | 8.03 | 38.1 | 4.74 | −19.8 | 1531 | 570.8 | 0.93 | 54.2 | 2.32 | 87.8 |
| S0G0.2L6 | 34.24 | −0.3 | 6.53 | 12.3 | 5.25 | −11.3 | 297 | 30.3 | 0.72 | 19.0 | 1.79 | 44.5 |
| S0.4G0.2L6 | 36.57 | 6.4 | 7.18 | 23.6 | 5.09 | −13.9 | 480 | 110.4 | 0.91 | 50.0 | 1.94 | 57.1 |
| S0.8G0.2L6 | 38.57 | 12.3 | 8.26 | 42.2 | 4.67 | −21.0 | 1063 | 365.7 | 0.90 | 49.4 | 2.44 | 97.6 |
| S1.2G0.2L6 | 42.55 | 23.8 | 8.78 | 51.0 | 4.85 | −18.0 | 1755 | 669.2 | 0.96 | 58.3 | 2.63 | 112.8 |
| S0G0.4L6 | 34.77 | 1.2 | 7.27 | 25.1 | 4.78 | −19.1 | 333 | 46.0 | 0.80 | 32.2 | 1.71 | 38.5 |
| S0.4G0.4L6 | 34.77 | 1.2 | 7.40 | 27.4 | 4.70 | −20.6 | 736 | 222.4 | 0.91 | 51.4 | 1.88 | 51.8 |
| S0.8G0.4L6 | 40.05 | 16.6 | 8.48 | 45.9 | 4.72 | −20.1 | 1175 | 415.0 | 0.89 | 47.7 | 2.31 | 87.0 |
| S1.2G0.4L6 | 36.87 | 7.3 | 8.84 | 52.0 | 4.17 | −29.4 | 1737 | 661.2 | 0.98 | 61.6 | 2.70 | 118.4 |
| S0G0.6L6 | 35.26 | 2.6 | 7.31 | 25.7 | 4.83 | −18.4 | 351 | 53.6 | 0.90 | 49.5 | 1.95 | 57.8 |
| S0.4G0.6L6 | 39.53 | 15.0 | 7.59 | 30.5 | 5.21 | −11.9 | 903 | 295.6 | 1.08 | 79.5 | 2.07 | 67.5 |
| S0.8G0.6L6 | 37.58 | 9.4 | 8.75 | 50.5 | 4.30 | −27.3 | 1283 | 462.1 | 1.09 | 80.3 | 2.39 | 93.4 |
| S1.2G0.6L6 | 33.73 | −1.8 | 8.73 | 50.1 | 3.87 | −34.6 | 1798 | 687.9 | 1.07 | 77.8 | 2.69 | 117.7 |
| S0G0.2L12 | 35.68 | 3.8 | 6.09 | 4.8 | 5.86 | −0.9 | 298 | 30.6 | 0.91 | 51.3 | 1.31 | 5.6 |
| S0.4G0.2L12 | 37.95 | 10.4 | 7.37 | 26.7 | 5.15 | −12.8 | 755 | 230.9 | 1.01 | 67.4 | 1.63 | 31.6 |
| S0.8G0.2L12 | 39.81 | 15.9 | 7.99 | 37.5 | 4.98 | −15.8 | 1331 | 483.3 | 0.94 | 56.3 | 2.25 | 82.2 |
| S1.2G0.2L12 | 41.59 | 21.0 | 9.06 | 55.9 | 4.59 | −22.4 | 1727 | 656.8 | 1.02 | 68.6 | 2.24 | 80.8 |
| S0G0.4L12 | 36.36 | 5.8 | 6.71 | 15.4 | 5.42 | −8.3 | 267 | 16.9 | 0.90 | 49.3 | 1.33 | 7.2 |
| S0.4G0.4L12 | 38.49 | 12.0 | 7.88 | 35.5 | 4.89 | −17.4 | 901 | 294.7 | 0.99 | 63.2 | 1.71 | 38.6 |
| S0.8G0.4L12 | 38.99 | 13.5 | 8.07 | 38.8 | 4.83 | −18.3 | 1403 | 514.6 | 0.95 | 56.7 | 2.26 | 82.3 |
| S1.2G0.4L12 | 43.60 | 26.9 | 9.59 | 64.9 | 4.55 | −23.1 | 1998 | 775.6 | 1.16 | 92.0 | 2.57 | 107.6 |
| S0G0.6L12 | 37.18 | 8.2 | 6.83 | 17.4 | 5.45 | −7.9 | 325 | 42.5 | 0.95 | 58.0 | 1.43 | 15.6 |
| S0.4G0.6L12 | 39.90 | 16.1 | 8.16 | 40.4 | 4.89 | −17.3 | 942 | 312.9 | 0.97 | 61.1 | 1.73 | 39.9 |
| S0.8G0.6L12 | 38.02 | 10.7 | 9.01 | 55.0 | 4.22 | −28.6 | 1357 | 494.7 | 1.09 | 80.1 | 2.05 | 65.5 |
| S1.2G0.6L12 | 40.28 | 17.2 | 9.19 | 58.1 | 4.38 | −25.9 | 1702 | 645.9 | 1.13 | 86.7 | 2.29 | 85.5 |

* RV: representative value; PC: percentage changes.

3.3.1. Compressive Strength

As shown in Table 5, when the SF contents were 0 and 0.4%, the compressive strength increased with the GF content. When the SF content was greater than 0.4%, the compressive strength first increased and then decreased with increasing GF content. Specifically, when only GFs were added at 0.6%, the 6 mm and 12 mm GFs resulted in the largest increase in the compressive strength, which was 2.6 and 8.2%, respectively. When only 1.2% SFs were added, the greatest gain in compressive strength was 10.9%. However, when the 12 mm GF content was 0.4% and SF content was 1.2%, the largest gain in compressive strength was 26.9%. Therefore, although the separate addition of the two fibres can improve the compressive strength of RRC, the combination of GFs and SFs resulted in the largest compressive strength.

3.3.2. Flexural Strength

The flexural strength of the fracture test was calculated using Equation (1) and is shown in Table 5 and Figure 7. When the SF content was less than 1.2%, the flexural strength of each series increased with the GF content; however, the growth rate decreased. In this case, the flexural strength of the RRC reached its maximum at a GF content of 0.6%. When the SF content was 1.2%, the flexural strength first increased and then decreased with an increase in the GF content. The flexural strength of the RRC reached a maximum at a GF content of 0.4%, which was similar to 0.3–0.6% in the literature [44]. Specifically, when only GFs were added at 0.6%, the 6 mm and 12 mm GFs resulted in the largest increase in the flexural strength, which was 25.7 and 17.4%, respectively. For the specimens with SFs, 6 mm and 12 mm GFs make the highest improvements in flexural strength, which were 52.0 and 64.9%, respectively, when the SF content was 1.2% and the GF content was 0.4%.

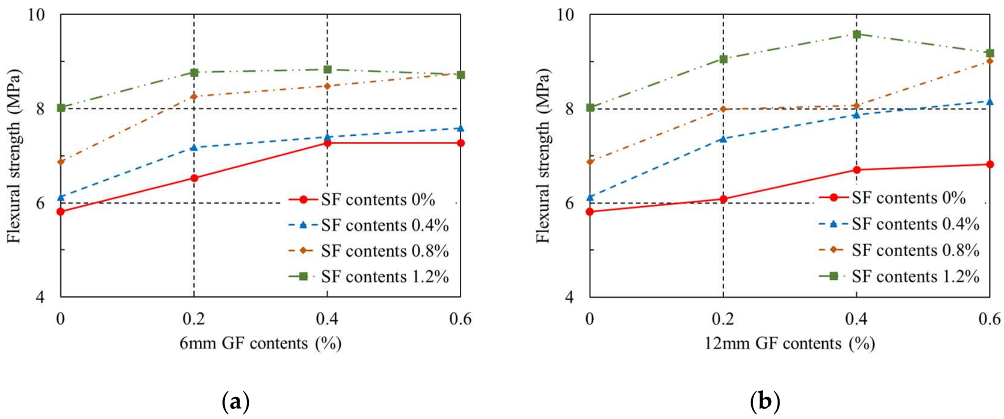


**Figure 7.** Flexural strength: (**a**) 6 mm GF; (**b**) 12 mm GF.

In addition, when only 1.2% SF was added, the greatest increase in flexural strength was 38.1%. For the specimen with only 12 mm GF, the growth rate of the flexural strength reached a maximum of 17.4% when the GF content was 0.6%. However, in the case of hybrid fibres, the growth rate of the flexural strength reached a maximum of 64.9% when the SF content was 1.2% and the 12 mm GF content was 0.4%. Therefore, the separate addition of SFs and GFs can improve the flexural strength of the RRC. The combination of GFs and SFs resulted in the largest flexural strength. The positive mixing effect was caused by the different properties of the SFs and GFs. At the initial stage, a larger quantity of GFs effectively reduces the stress concentration at the microcrack tip. Therefore, the stress can be redistributed and more matrix materials can be used, improving the strength of the RRC specimen. Due to the significant impact of GFs on the workability of RRC, it is not advisable to exceed 0.4% of GF content when the total volume fraction of hybrid fibres is large. Due to the high strength and elastic modulus of SFs, a skeleton was formed inside the concrete. Simultaneously, the SFs played a bridging role when a macroscopic crack appeared until the SFs were pulled out and failed.

### 3.3.3. Brittleness Coefficient

The brittleness coefficient, defined as the ratio of the compressive strength to the flexural strength, is an important index for RRC subjected to tensile failure. RRC with larger brittleness coefficients exhibited greater brittleness. The brittleness coefficients of the RRC are listed in Table 5 and Figure 8. For the specimens without adding SFs, when the GF content was 0.4%, 6 and 12 mm GFs make the maximum decrease in brittleness coefficient, which were −19.1 and −8.3%, respectively. For the specimens with SFs, when the 6 mm GF content and SF content was 0.6% and 1.2%, respectively, the maximum decrease in the brittleness coefficient was −34.6%. When the 12 mm GF content and SF content was 0.6% and 0.8%, respectively, the maximum decrease in brittleness coefficient was −28.6%. Overall, the addition of fibres can reduce the brittleness coefficient of the RRC. It can be noted that when 12 mm GFs and SFs were added together, the brittleness coefficient only slightly decreased with the increase in GF content, when the content of GF was larger than 0.4%. Therefore, the relationship between the brittleness coefficient and the GF content is quite complex. For 6 mm GF, the optimal content was 0.4–0.6%. For 12 mm GF, the optimal dosage was 0.4%.

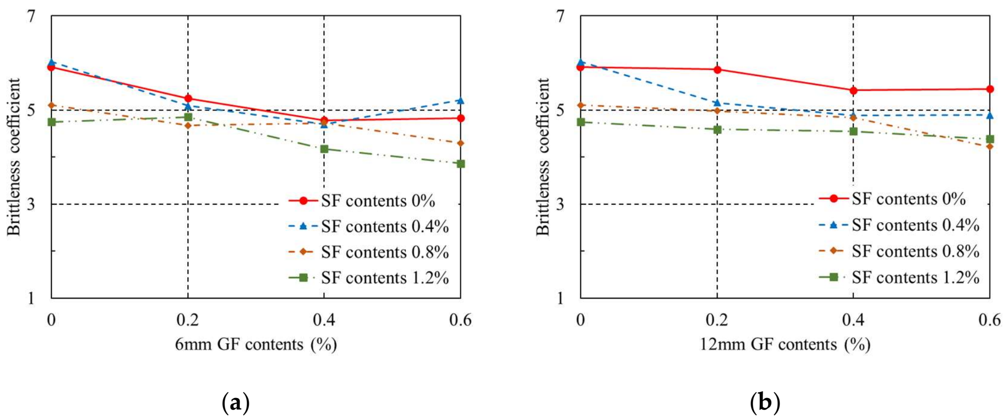


**Figure 8.** Brittleness coefficient: (**a**) 6 mm GF; (**b**) 12 mm GF.

### 3.3.4. Fracture Energy

As the most useful material parameter in the analysis of cracked concrete structures, the fracture energy was calculated using Equation (2) [45]. It is shown in Table 5 and Figure 9. The fracture energy reflects the amount of energy dissipated by the RRC fracture. When only GFs were added, the fracture energy increased slightly with increasing GF content. When only 0.6% GFs were added, the 6 and 12 mm GFs resulted in the highest improvements in the fracture energy, which were 53.6% and 42.5%, respectively. When only SFs were added, the fracture energy increased significantly with increasing SF content, with the greatest improvement being 570.8%. When the 6 mm GF content and SF content was 0.6% and 1.2%, respectively, the maximum increase in the fracture energy was 687.9%. When the 12 mm GF content and SF content was 0.4% and 1.2%, respectively, the maximum increase in fracture energy was 775.6%. Overall, the fracture energy increased with the increase in the content of two types of fibres, especially SFs. The reason was that even at lower fibre content, the softening part of the load–deflection curves of RRC containing SFs were longer [33]. The 12 mm GFs caused a greater increase in fracture energy than the 6 mm GFs. This was because the propagation of cracks typically avoids the area where the fibres were located, and longer GFs make it more difficult for cracks to avoid them.

In addition, when only 1.2% SFs were added, the greatest gain in fracture energy was 570.8%. For the specimen with only 12 mm GF, the growth rate of the fracture energy reached a maximum of 42.5% when the GF content was 0.6%. However, in the case of hybrid fibres, the growth rate of the fracture energy reached a maximum of 775.6% when the content of SF was 1.2% and the content of 12 mm GF was 0.4%. Therefore, although both SFs and GFs can increase the fracture energy of RRC, SFs play a major role. According to

Figure 9, without adding SFs, the lines became gentler with increasing GF content. However, when SFs were added, the slope of the lines increased, indicating that the two fibres had a positive mixing effect. This was because brittle GFs fail quickly after the appearance of macroscopic cracks. GFs alone cannot effectively limit the crack development after peak loads. When SFs were added, SFs prevented the rapid development of macroscopic cracks. The specimens containing SFs had more tortuous cracks, indicating that more GFs and RRC played a role in increasing the energy consumed for crack development. The failure modes of the RRC confirmed this, as described in Section 3.1.

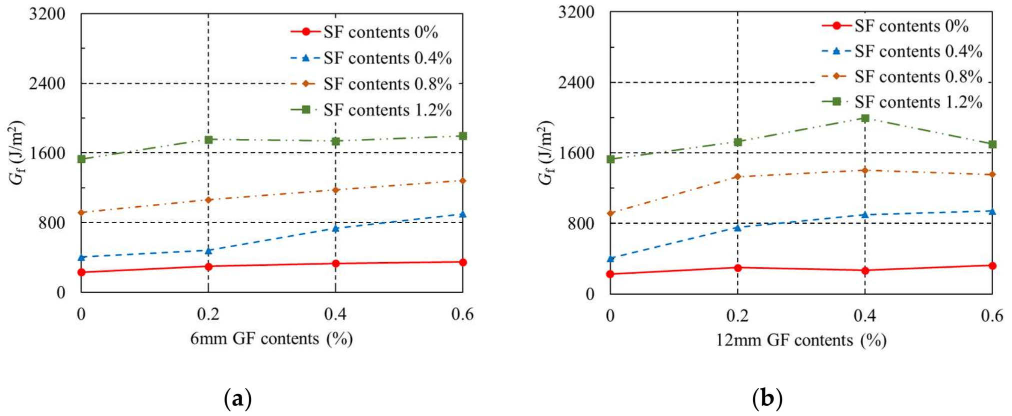


**Figure 9.** Fracture energy: (**a**) 6 mm GF; (**b**) 12 mm GF.

### 3.3.5. Initial Fracture Toughness

The initial fracture toughness results are presented in Table 5 and Figure 10. Equation (3) shows that the initial fracture toughness is proportional to the cracking load. Therefore, the effect of SFs and GFs on the cracking load was equal to their effect on the initial fracture toughness. In general, the initial fracture toughness of the RRC was increased by the inclusion of fibres. When only 1.2% SFs was added, the highest gain in the initial fracture toughness was 54.2%. When only 0.6% GFs were added, the 6 mm and 12 mm GFs resulted in the highest improvement in the initial fracture toughness, which was 49.5 and 58.0%, respectively. When the 12 mm GF content and SF content was 0.4% and 1.2%, respectively, the initial fracture toughness gained a maximum increase of 92.0%. Before the RRC cracked, the RRC and fibres were synergistically deformed by the adhesive force. Compared with RRC without fibres, the high elastic modulus of SFs allows RRC to withstand greater loads under the same deformation, thereby increasing the cracking load. The increase in initial fracture toughness was not significant with the increase in SF content. Literature [41] introduced 1% SF into concrete, which only increased the initial fracture toughness by 2.6%. Simultaneously, because of the higher quantity of GFs in the same content, the formation and development of microscopic cracks were limited by the GFs better. Therefore, GF seems to contribute more significantly to the initial fracture toughness than SF. Compared with single fibres, hybrid fibres were more effective in the enhancement of the initial fracture toughness of RRC.

### 3.3.6. Unstable Fracture Toughness

The unstable fracture toughness results are listed in Table 5 and shown in Figure 11. In general, the unstable fracture toughness of RRC increased with an increase in the SF content but only slightly increased through increasing the content of GF. When only 1.2% SFs were added, the greatest gain in the unstable fracture toughness was 87.8%. When only 0.6% GFs were added, both lengths of GFs resulted in the highest improvements in the unstable fracture toughness, which were 57.8% and 15.6%, respectively. When the 6 mm GF content and SF content was 0.4% and 1.2%, respectively, the maximum increase in the unstable fracture toughness was 118.4%. Compared to the initial fracture toughness, SFs had a more significant improvement in unstable fracture toughness. This conclusion can also be drawn from literature [41]. For the RRC specimens reinforced with the two types of fibres, the increase in the unstable fracture toughness was not significant with the increase in the GF content. This was because unstable fracture toughness is the critical point at which cracks develop from stability to instability. The bridging effect of the GFs mainly occurs in the microcrack stage. After the appearance of macroscopic cracks, most of GFs quickly fail. Therefore, the amount of GF content has little effect on the unstable fracture toughness. At this time, the SFs play a major bridging role, slowing down the development of macroscopic cracks, and thereby improving the unstable fracture toughness of the RRC.

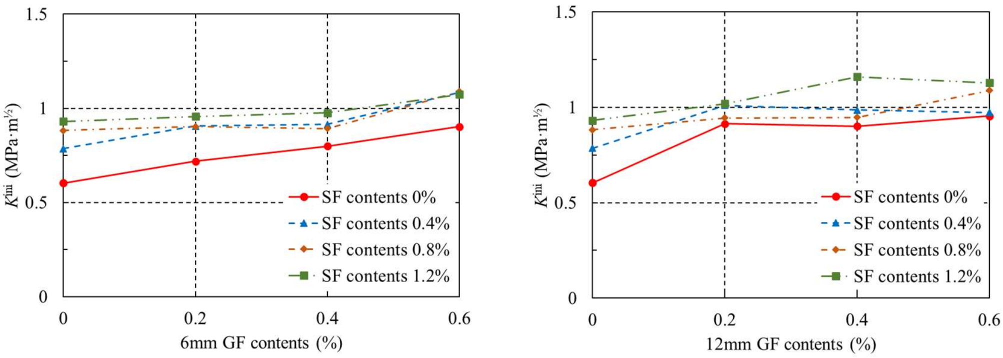


(**a**) (**b**)

**Figure 10.** Initial fracture toughness: (**a**) 6 mm GF; (**b**) 12 mm GF.

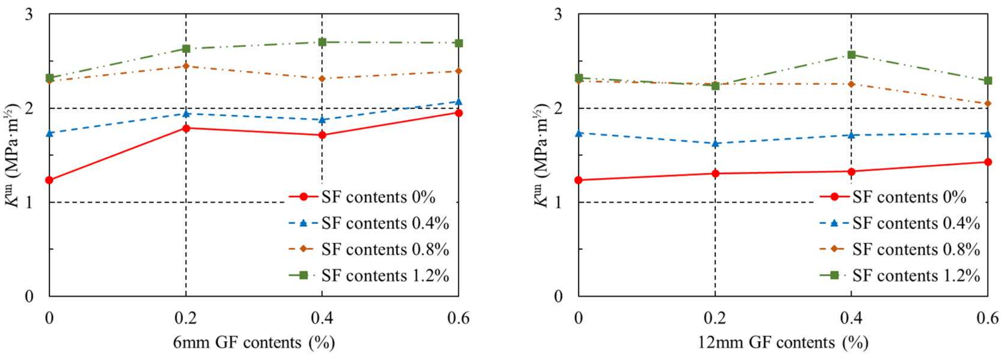


(**a**) (**b**)

**Figure 11.** Unstable fracture toughness: (**a**) 6 mm GF; (**b**) 12 mm GF.

## 4. Mechanism Analysis

Through the analysis of the failure modes and various indices, it can be inferred that the incorporation of SFs is useful for improving the fracture performance of RRC. Before the cracking load, there was a strong bond between the SFs and RRC. The high elastic modulus and tensile strength of SFs can improve the bearing capacity of RRC, thereby improving the peak and cracking loads. As illustrated in Figure 12a, after the peak load, because the tensile strength of the SFs was greater than the bonding strength with the RRC, the SFs were always pulled out rather than broken. Previous literature has indicated that, until the tensile deformation of SF-reinforced concrete reaches 1/4 of the fibre length, the tensile stress decreases to 0 [37]. Therefore, the SFs located at the tip of the crack can still play a bridging role so that the concrete on both sides of the crack can continue to bear the load. As the SFs were pulled out, the neutral axis and the tip of the crack slowly developed upward. The energy consumed by this process is characterised by an increase in fracture energy.

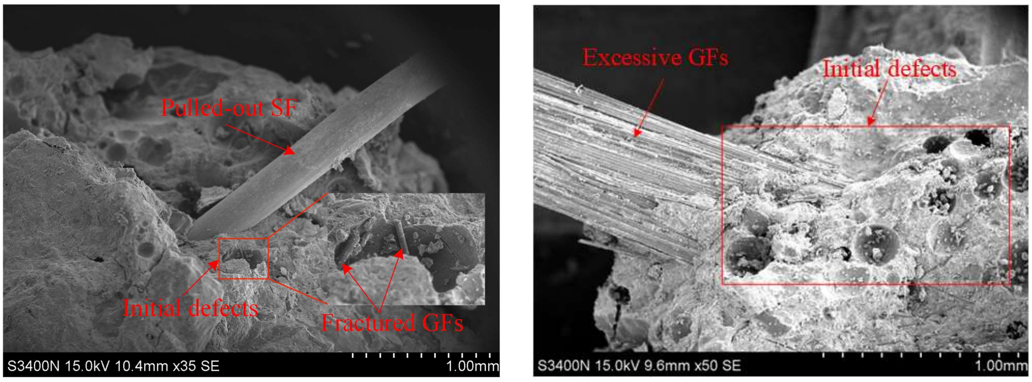


(**a**) (**b**)

**Figure 12.** SEM test results: (**a**) the failure modes of fibres at the crack; (**b**) initial defects caused by excessive GFs.

The influence of the GFs on the fracture performance of RRC mainly occurred before the cracking load. As RRC is a heterogeneous material, there may be certain initial internal defects. When RRC is subjected to external loads, microcracks usually develop from the initial defect and eventually interconnect into macroscopic cracks. In particular, when excessive GFs were added, the poor workability increased the initial defects of the RRC, as shown in Figure 12b. Therefore, the GF content should not be excessively high. When an appropriate GF content is used, the fracture performance of the RRC can be effectively improved, and the workability of the RRC is less affected. Because there were significantly more GFs than SFs at a given fibre content, the formation and growth of microcracks may be efficiently suppressed. Because GFs are brittle materials and microcracks are present on the glass surface, their strength is generally lower than the theoretical strength. Therefore, most of the GFs located in the macroscopic cracks broke after the cracking load. Therefore, the GFs had no significant bridging effect on the descending segment after the peak load.

The fracture properties of the RRC were maximised by the combined addition of SFs and GFs. This indicates that the SFs and GFs had a positive mixing effect on the fracture properties of RRC. In the preliminary loading period, the GFs was useful for inhibiting the formation and growth of microcracks. As the load continued to increase, the microcracks interconnected to form macroscopic cracks. At this point, the bridging effect of the SFs slowed the development of cracks. The two parts bridged by the SFs could continue to bear the load, allowing more RRC and GFs to work. This was verified using fracture energies. As shown in Figure 9, after the addition of SFs, the fracture energy increased more significantly with an increase in GF content. However, the variation in the experimental results is complex because the fibre content has an important impact on the workability of fresh RRC. Further studies are required to elucidate the mechanisms underlying HFRRRC.

## 5. Conclusions

Fracture experiments were conducted on 28 different concrete mixes in order to examine the effects of SFs and GFs on the fracture characteristics of RRC. Analysis was performed on the failure mechanism, load–deflection curves, flexural strength, fracture energy, brittleness coefficient, initial fracture toughness, and unstable fracture toughness. The test findings supported the following deductions:

(1) The fractured specimens without SFs were damaged by vertical cracks and their crack widths were smaller. The two GF lengths had no significant effect on the final morphology of the cracks. With the addition of the SFs, the cracks became more curved as the crack width increased. The SFs primarily played a bridging role after RRC cracking. At this point, the GFs located in the cracks had failed.

(2) In general, the peak load increased with increasing dosages of both fibres. However, with 1.2% SFs, the excessive addition of GFs decreased the peak load. For specimens

with only GFs, the peak deflection increased and then decreased, indicating brittle damage. The addition of SFs significantly improved the post-peak deformation capacity and smoothed the descending section of the load–deflection curves. The specimens of the 12 mm GFs series exhibited a greater enhancement of the deformation capacity when SFs were added.

(3) When only SFs were added, the maximum increases or decreases in flexural strength, brittleness coefficient, fracture energy, initial fracture toughness, and unstable fracture toughness with increasing SF content were 38.1, −19.8, 570.8, 54.2, and 87.8%, respectively. When only GFs were added, the maximum increases or decreases in the above-mentioned indices with increasing GF content were 25.7, −19.1, 53.6, 58.0, and 57.8%, respectively. When SFs and GFs were added together, the maximum increases and decreases in the above-mentioned indices with increasing GF content were 64.9, −34.6, 775.6, 92.0, and 118.4%, respectively. Thus, although the addition of SFs or GFs alone also improved the mechanical performance indices of the RRC, the combination of SFs and GFs produced the most significant improvements.

(4) In this study, the optimum GF content was found to be 0.4–0.6%. It decreases with increasing SF content ensuring the workability of the RRC.

(5) The mechanism for the positive mixing effect of SFs and GFs was that they acted at different stages during the fracture test. A large number of GFs restricted the development of microcracks in the early stages of the test. After the RRC cracked, which caused the GFs to fail, the SFs still acted as bridges.

(6) To prevent the cracking of rubber concrete pavement caused by external factors, adding SFs and GFs together is an effective solution. Before practical application, more performance indicators need to be quantitatively analysed. The durability and impact resistance of HFRRRC still needs to be studied.

**Author Contributions:** Conceptualisation, L.L. and X.L.; methodology, X.L. and F.L.; software, Z.P.; validation, Z.C., H.L. and Z.W.; formal analysis, W.L.; investigation, H.Z.; resources, H.L. and Z.W.; data curation, Z.P.; writing—original draft preparation, X.L.; writing—review and editing, W.L.; visualisation, H.Z.; supervision, L.L.; project administration, Z.C.; funding acquisition, L.L. and F.L. All authors have read and agreed to the published version of the manuscript.

**Funding:** This research was funded by the National Natural Science Foundation of China, grant numbers 12072080 and 12032009.

**Data Availability Statement:** The original contributions presented in the study are included in the article, further inquiries can be directed to the corresponding authors.

**Conflicts of Interest:** Author Zhuangwei Chen was employed by the company Guangdong Henghui Construction Group Co., Ltd. Authors Hongming Li and Zhichao Wu were employed by the company Guangdong Zhongdu Construction Group Co., Ltd. The remaining authors declare that the research was conducted in the absence of any commercial or financial relationships that could be construed as a potential conflict of interest.

## References

1. Neupane, R.; Imjai, T.; Makul, N.; Garcia, R.; Kim, B.; Chaudhary, S. Use of recycled aggregate concrete in structural members: A review focused on Southeast Asia. *J. Asian Archit. Build.* **2023**, 1–24. [CrossRef]
2. Xiong, Z.; Mai, G.; Pan, Z.; Chen, Z.; Jian, J.; Wang, D.; Ling, Z.; Li, L. Synergistic effect of expansive agents and glass fibres on fatigue bending performance of seawater sea sand concrete. *Constr. Build. Mater.* **2024**, *421*, 135665. [CrossRef]
3. Asaro, L.; Gratton, M.; Seghar, S.; Hocine, N.A. Recycling of Rubber Wastes by Devulcanization. *Resour. Conserv. Recy.* **2018**, *133*, 250–262. [CrossRef]
4. Li, Y.; Chai, J.; Wang, R.; Zhou, Y.; Tong, X. A Review of the Durability-Related Features of Waste Tyre Rubber as a Partial Substitute for Natural Aggregate in Concrete. *Buildings* **2022**, *12*, 1975. [CrossRef]
5. Tang, Y.; Feng, W.; Chen, Z.; Nong, Y.; Guan, S.; Sun, J. Fracture behavior of a sustainable material: Recycled concrete with waste crumb rubber subjected to elevated temperatures. *J. Clean. Prod.* **2021**, *318*, 128553. [CrossRef]
6. Gupta, T.; Chaudhary, S.; Sharma, R.K. Assessment of Mechanical and Durability Properties of Concrete Containing Waste Rubber Tire as Fine Aggregate. *Constr. Build. Mater.* **2014**, *73*, 562–574. [CrossRef]

7. Pham, T.M.; Renaud, N.; Pang, V.; Shi, F.; Hao, H.; Chen, W. Effect of Rubber Aggregate Size on Static and Dynamic Compressive Properties of Rubberized Concrete. *Struct. Concr.* **2021**, *23*, 2510–2522. [CrossRef]
8. Guo, S.; Dai, Q.; Si, R.; Sun, X.; Lu, C. Evaluation of Properties and Performance of Rubber-modified Concrete for Recycling of Waste Scrap Tire. *J. Clean. Prod.* **2017**, *148*, 681–689. [CrossRef]
9. Xie, J.; Guo, Y.; Liu, L.; Xie, Z. Compressive and flexural behaviours of a new steel-fibre-reinforced recycled aggregate concrete with crumb rubber. *Constr. Build. Mater.* **2015**, *79*, 263–272. [CrossRef]
10. Pacheco-Torres, R.; Cerro-Prada, E.; Escolano, F.; Varela, F. Fatigue Performance of Waste Rubber Concrete for Rigid Road Pavements. *Constr. Build. Mater.* **2018**, *176*, 539–548. [CrossRef]
11. Msallam, M.; Asi, I. Improvement of Local Asphalt Concrete Binders Using Crumb Rubber. *J. Mater. Civil Eng.* **2018**, *30*, 04018048. [CrossRef]
12. Chen, J.; Zhuang, J.; Shen, S.; Dong, S. Experimental Investigation on the Impact Resistance of Rubber Self-compacting Concrete. *Structures* **2022**, *39*, 691–704. [CrossRef]
13. Gupta, T.; Tiwari, A.; Siddique, S.; Sharma, R.K.; Chaudhary, S. Response Assessment under Dynamic Loading and Microstructural Investigations of Rubberized Concrete. *J. Mater. Civil Eng.* **2017**, *29*, 04017062. [CrossRef]
14. Guo, X.; Xiong, Z.; Luo, Y.; Qiu, L.; Liu, J. Experimental Investigation on the Semi-rigid Behaviour of Aluminium Alloy Gusset Joints. *Thin Wall. Struct.* **2015**, *87*, 30–40. [CrossRef]
15. Xiong, Z.; Guo, X.; Luo, Y.; Zhu, S. Elasto-plastic Stability of Single-layer Reticulated Shells with Aluminium Alloy Gusset Joints. *Thin Wall. Struct.* **2017**, *115*, 163–175. [CrossRef]
16. Fang, Z.; Wu, J.; Xian, B.; Zhao, G.; Fang, S.; Ma, Y.; Jiang, H. Shear Performance and Design Recommendations of Single Embedded Nut Bolted Shear Connectors in Prefabricated Steel–UHPC Composite Beams. *Steel Compos. Struct.* **2024**, *50*, 319–336. [CrossRef]
17. Lin, J.; Luo, R.; Su, J.; Guo, Y.; Chen, W. Coarse synthetic fibers (PP and POM) as a replacement to steel fibers in UHPC: Tensile behavior, environmental and economic assessment. *Constr. Build. Mater.* **2024**, *412*, 134654. [CrossRef]
18. Fang, Z.; Wu, J.; Xu, X.; Ma, Y.; Fang, S.; Zhao, G.; Jiang, H. Grouped rubber-sleeved studs–UHPC pocket connections in prefabricated steel–UHPC composite beams: Shear performance under monotonic and cyclic loadings. *Eng. Struct.* **2024**, *305*, 117781. [CrossRef]
19. He, L.; Cai, H.; Huang, Y.; Ma, Y.; Bergh, W.V.D.; Gaspar, L.; Valentin, J.; Vasiliev, Y.E.; Kowalski, K.J.; Zhang, J. Research on the Properties of Rubber Concrete Containing Surface-modified Rubber Powders. *J. Build. Eng.* **2021**, *35*, 101991. [CrossRef]
20. Xu, Y.; Wang, J.; Zhang, P.; Guo, J.; Hu, S. Enhanced Effect and Mechanism of Colloidal Nano-$SiO_2$ Modified Rubber Concrete. *Constr. Build. Mater.* **2023**, *378*, 131203. [CrossRef]
21. Kang, J.; Liu, Y.; Yuan, J.; Chen, C.; Wang, L.; Yu, Z. Effectiveness of Surface Treatment on Rubber Particles towards Compressive Strength of Rubber Concrete: A Numerical Study on Rubber-cement Interface. *Constr. Build. Mater.* **2022**, *350*, 128820. [CrossRef]
22. Zhu, H.; Xiong, Z.; Song, Y.; Zhou, K.; Su, Y. Effect of Expansion Agent and Glass Fiber on the Dynamic Splitting Tensile Properties of Seawater–Sea-Sand Concrete. *Buildings* **2024**, *14*, 217. [CrossRef]
23. Pan, Z.; Liu, F.; Li, H.; Li, X.; Wang, D.; Ling, Z.; Zhu, H.; Zhu, Y. Performance Evaluation of Thermal Insulation Rubberized Mortar Modified by Fly Ash and Glass Fiber. *Buildings* **2024**, *14*, 221. [CrossRef]
24. Wang, X.; Shao, J.; Wang, J.; Ma, M.; Zhang, B. Influence of Basalt Fiber on Mechanical Properties and Microstructure of Rubber Concrete. *Sustainability* **2022**, *14*, 12517. [CrossRef]
25. Zhen, H.; Xiong, Z.; Song, Y.; Li, L.; Qiu, Y.; Zou, X.; Chen, B.; Chen, D.; Liu, F.; Ji, Y. Early Mechanical Performance of Glass Fibre-reinforced Manufactured Sand Concrete. *J. Build. Eng.* **2024**, *83*, 108440. [CrossRef]
26. Merli, R.; Preziosi, M.; Acampora, A.; Lucchetti, M.C.; Petrucci, E. Recycled Fibers in Reinforced Concrete: A Systematic Literature Review. *J. Clean. Prod.* **2020**, *248*, 119207. [CrossRef]
27. Gong, C.; Kang, L.; Zhou, W.; Liu, L.; Lei, M. Tensile Performance Test Research of Hybrid Steel Fiber—Reinforced Self-Compacting Concrete. *Materials* **2023**, *16*, 1114. [CrossRef]
28. Bhosale, A.; Rasheed, M.A.; Prakash, S.S.; Raju, G. A study on the efficiency of steel vs. synthetic vs. hybrid fibers on fracture behavior of concrete in flexure using acoustic emission. *Constr. Build. Mater.* **2019**, *199*, 256–268. [CrossRef]
29. Gong, Y.; Song, J.; Zhang, Y.; Jiang, T. Sustainable Utilization of Foundry Waste: Cracking Property Analysis of Basalt Fiber-Reinforced Rubber Concrete. *J. Mater. Civil Eng.* **2023**, *35*, 04023181. [CrossRef]
30. Zhao, Y.; Bi, J.; Wang, Z.; Huo, L.; Guan, J.; Zhao, Y.; Sun, Y. Numerical Simulation of the Casting Process of Steel Fiber Reinforced Self-compacting Concrete: Influence of Material and Casting Parameters on Fiber Orientation and Distribution. *Constr. Build. Mater.* **2021**, *312*, 125337. [CrossRef]
31. Wang, J.; Dai, Q.; Guo, S.; Si, R. Study on Rubberized Concrete Reinforced with Different Fibers. *ACI Mater. J.* **2019**, *116*, 21–31. [CrossRef]
32. Gültekin, A.; Beycioğlu, A.; Arslan, M.; Serdar, A.; Dobiszewska, M.; Ramyar, K. Fresh Properties and Fracture Energy of Basalt and Glass Fiber–Reinforced Self-Compacting Concrete. *J Mater. Civil. Eng.* **2021**, *34*, 04021406. [CrossRef]
33. Muhyaddin, G. Mechanical and fracture characteristics of ultra-high performance concretes reinforced with hybridization of steel and glass fibers. *Heliyon* **2023**, *9*, e17926. [CrossRef] [PubMed]
34. Akça, K.R.; Çakır, Ö.; Ipek, M. Properties of Polypropylene Fiber Reinforced Concrete using Recycled Aggregates. *Constr. Build. Mater.* **2015**, *98*, 620–630. [CrossRef]

35. *GB/T 14684-2011*; Sand for Construction. General Administration of Quality Supervision. Inspection and Quarantine: Beijing, China, 2011.
36. *GB/T 14685-2011*; Pebble and Crushed Stone for Construction. General Administration of Quality Supervision. Inspection and Quarantine: Beijing, China, 2011.
37. *DL/T 5332-2005*; Norm for Fracture Test of Hydraulic Concrete. Inspection and Quarantine: Beijing, China, 2005.
38. *ASTM C39/C39M-21*; Standard Test Method for Compressive Strength of Cylindrical Concrete Specimens. ASTM International: West Conshohocken, PA, USA, 2021.
39. Xu, S.; Reinhardt, H.W. A Simplified Method for Determining Double-K Fracture Parameters for Three-point Bending Tests. *Int. J. Fract.* **2000**, *104*, 181–209. [CrossRef]
40. Li, X.; Dong, W.; Wu, Z.; Chang, Q. Experimental Investigation on Double-K Fracture Parameters for Small Specimens of Concrete. *Eng. Mech.* **2010**, *27*, 166–171. (In Chinese)
41. Xie, J.; Li, J.; Lu, Z.; Li, Z.; Fang, C.; Huang, L.; Li, L. Combination Effects of Rubber and Silica Fume on the Fracture Behaviour of Steel-fibre Recycled Aggregate Concrete. *Constr. Build. Mater.* **2019**, *203*, 164–173. [CrossRef]
42. Abdallah, M.A.; Elakhras, A.A.; Reda, R.M.; Sallam, H.E.-D.M.; Moawad, M. Applicability of CMOD to Obtain the Actual Fracture Toughness of Rightly-Cracked Fibrous Concrete Beams. *Buildings* **2023**, *13*, 2010. [CrossRef]
43. Soetens, T.; Matthys, S. Different Methods to Model the Post-cracking Behaviour of Hooked-end Steel Fibre Reinforced Concrete. *Constr. Build. Mater.* **2014**, *73*, 458–471. [CrossRef]
44. Akbari, J.; Abed, A. Experimental evaluation of effects of steel and glass fibers on engineering properties of concrete. *Frat. Integrita Strut.* **2020**, *54*, 116–127. [CrossRef]
45. Karihaloo, B.; Abdalla, H.; Imjai, T. A simple method for determining the true specific fracture energy of concrete. *Mag. Concr. Res.* **2003**, *55*, 471–481. [CrossRef]